Available online at www.sciencedirect.com

ScienceDirect

Advances in Space Research xxx (2015) xxx–xxx

ADVANCES IN SPACE RESEARCH (a COSPAR publication)

www.elsevier.com/locate/asr

Spectral pathways for exploration of secondary uranium: An investigation in the desertic tracts of Rajasthan and Gujarat, India

Rishikesh Bharti, R. Kalimuthu, D. Ramakrishnan *

Department of Earth Sciences, Indian Institute of Technology Bombay, Powai, Mumbai 400076, Maharashtra, India

Received 27 February 2015; received in revised form 3 July 2015; accepted 14 July 2015

Abstract

This study aims at identifying potential zones of secondary uranium enrichment using hyperspectral remote sensing, γ-ray spectrometry, fluorimetry and geochemical techniques in the western Rajasthan and northern Gujarat, India. The investigated area has suitable source rocks, conducive past-, and present-climate that can facilitate such enrichment. This enrichment process involves extensive weathering of uranium bearing source rocks, leaching of uranyl compounds in groundwater, and their precipitation in chemical deltas along with duricrusts like calcretes and gypcretes. Spatial distribution of groundwater calcretes (that are rich in Mg-calcite) and gypcretes (that are rich in gypsum) along palaeochannels and chemical deltas were mapped using hyperspectral remote sensing data based on spectral absorptions in 1.70 μm, 2.16 μm, 2.21 μm, 2.33 μm, 2.44 μm wavelength regions. Subsequently based on field radiometric survey, zones of U anomalies were identified and samples of duricrusts and groundwater were collected for geochemical analyses. Anomalous concentration of U (2345.7 Bq/kg) and Th (142.3 Bq/kg) are observed in both duricrusts and groundwater (U-1791 μg/l, Th-34 μg/l) within the palaeo-delta and river confluence. The estimated carnotite Solubility Index also indicates the secondary enrichment of U and the likelihood of occurrence of an unconventional deposit.

Keywords: Uranium exploration; Duricrust; Imaging spectroscopy; γ-Radiometry

1. Introduction

Compared to other sources of energy, uranium can produce large amounts of clean energy at very low cost and hence, it is one of the most sought after minerals. To fill the gap between demand and supply, there is a continuous endeavor to find various sources of uranium deposits. So far, economically viable deposits are exploited from conventional deposits (e.g. sandstone type, iron-oxide breccias type, and Proterozoic unconformity type) only. However with the depleting resources, the unconventional deposits (e.g. surficial type, phosphate type and black shale type) will be the main focus for near future. The recent discovery of huge near-surface, unconventional uranium deposits associated with palaeochannels and playas in Australia, South Africa and USA has attracted the attention of geoscientists globally (Carlisle, 1978; Hambleton-Jones and Toen, 1978; Mann and Deutscher, 1978; Arakel, 1988; Hartleb, 1988; Hou et al., 2007; Mann and Horwitz, 2007; Bowell et al., 2008; Noble et al., 2011). Carnotite ($K(UO_2)_2(VO_4)_2.3H_2O$), the predominant uranium mineral in these deposits is associated with calcite, gypsum, dolomite and ferric oxide precipitated from the groundwater (Carlisle, 1983; Arakel, 1988; Bowell et al., 2008; Hou et al., 2007). For uranium to undergo enrichment in secondary environment, factors such as prevalence of source rocks, warm humid palaeoclimate (to facilitate increased weathering rate), sluggish groundwater flow regime, arid to semi-arid recent climate (to promote evaporation),

* Corresponding author.
E-mail address: ramakrish@iitb.ac.in (D. Ramakrishnan).

http://dx.doi.org/10.1016/j.asr.2015.07.015
0273-1177/

geochemical barriers, and suitable physical–chemical conditions are necessary (Carlisle, 1983; Arakel, 1988; Bowell et al., 2008). It is evident from the Yeelirrie and Lake Maitland deposits that the calcretes (calcium carbonate duricrust) and gypcretes (gypsum duricrust) associated with palaeochannels are the most favorable hosts for secondary uranium (Mann and Deutscher, 1978; Carlisle, 1983; Arakel, 1988).

Duricrusts associated with palaeochannel and playa are amenable to mapping using hyperspectral (Hyperion) and multispectral (Landsat-8 (OLI), Landsat-7 ETM+, Landsat-TM and ASTER) satellite data. Conventionally, image processing techniques such as band ratio (Crosta and Mc.Moore, 1989; Tangestani and Moore, 2000; Ranjbar et al., 2004), supervised classification (Martínez-Montoya et al., 2010), linear mixture modeling (Bryant, 1996), data fusion with decorrelation stretching (Kavak, 2005) and spectral analysis (Crowley, 1993; Ramakrishnan et al., 2013; Bharti and Ramakrishnan, 2014) are extensively used to target such deposits based on characteristic spectral features. Spectral absorption features (particularly their position and shape) are unique to mineral species and are caused by electronic and vibration processes which reveal their chemistry (Burns, 1970; Hunt and Salisbury, 1970; Goetz et al., 1985). Hyperspectral remote sensing (HRS) is now a well-established and extensively used technique for mineral potential estimation and lithological discrimination (Ramakrishnan et al., 2013). Since absorption wavelengths are the key for identification and quantification of a mineral, an accurate wavelength calibration is critical and most important in analyzing the hyperspectral data. This warrants specialized data processing and analysis techniques such as atmospheric correction, dimensionality reduction, identification of pure endmembers and spectral analyses (Hubbard and Crowley, 2005; Kruse, 1996; Kusuma et al., 2012; Bharti and Ramakrishnan, 2014).

The host rocks in the present investigation, the calcretes, have characteristic absorption bands between 2.50–2.55 μm and 2.30–2.35 μm wavelength regions in addition to three other weak absorptions between 2.12–2.16 μm, 1.97–2 μm, and 1.85–1.87 μm (Hunt and Salisbury, 1970; Gaffey et al., 1993; Clark, 1999; Christensen et al., 2000; Gupta, 2003; Van-der-meer, 2004; Lagacherie et al., 2007; Bharti and Ramakrishnan, 2014). The important absorption features for uranium are located in 0.84 μm, 0.86 μm, 1.11 μm, 1.35–1.54 μm, 1.62 μm, 1.73 μm and 2.26 μm wavelength regions (Bates, 1965; Lévesque et al., 2001; Zhang, 2008). The gypcretes on the other hand have spectral absorption features at 1.70 μm, 2.21 μm, and 2.44 μm regions. These characteristic absorption features can be easily identified using image derived endmembers/lab measured spectra and airborne/spaceborne HRS data. Bharti and Ramakrishnan (2014) reported that the uranium concentration in calcretes correlate well with the high Mg-calcite content. In the investigated area, the high Mg-calcites are commonly observed with palaeochannels and playas having sluggish groundwater flow regime. As both gypsum and high Mg-calcites have typical spectral absorption positions, they are amenable to mapping using hyperspectral data. Once these duricrusts are identified, radiometric techniques such as gamma-ray spectrometry is widely used to explore the occurrence of radioactive materials (Gilmore, 2011). Gamma-ray energies can be measured in two different modes: (i) total count measurement (gamma-rays of all energies), and (ii) intensity and energy of radiation (IAEA-TECDOC-1363, 2003; Tsurikov, 2009). Total count measurement can give only the gross level of gamma radiation used to monitor or detect radiation anomalies whereas; γ-ray spectrometers can measure the γ-rays of various energies and produce a gamma energy spectrum. Based on the intensity (cps-count per second) of gamma radiation at particular energy levels in the spectrum, not only can the source radioisotope be identified, but its concentration may also be estimated (Gilmore, 2011; Butt and Mann, 1984; Heath et al., 1984; Raghuwanshi, 1992).

Since groundwater is the main transporting agent of uranyl compounds, it is also necessary to understand the mobility of various species of cations and anions in groundwater (Cameron et al., 2002; Tosheva et al., 2004; Leybourne and Cameron, 2007; Hou et al., 2007; Jobbágy et al., 2009). The significantly lower background concentrations and easy sample preparation make groundwater chemistry more informative than litho-geochemistry (Leybourne and Cameron, 2007). Various radiometric (liquid scintillation, alpha spectrometry, γ-ray spectrometry) and non-radiometric (spectrophotometry, fluorimetry, ICP-AES, ICP-MS) analytical techniques are extensively used for the analysis of uranium concentration in water samples (Lorber et al., 1987; Väisänen et al., 2000; Tosheva et al., 2004; Leybourne and Cameron, 2007; Jobbágy et al., 2009).

In this paper, a novel methodology involving imaging spectroscopy and conventional techniques are employed to identify the potential zones of secondary uranium enrichment in the western Rajasthan and northern Gujarat, India. Using imaging spectroscopy, the chemical delta and proxy (Mg-calcrete and gypcretes) minerals were targeted. Once the proxies were mapped, insitu Gamma-ray spectrometry and conventional geochemical studies of soil and water were carried out to delineate the potential zones.

2. Study area

The study area is bounded by latitudes 24–29° N and longitudes 70–76° E covering the northern parts of Gujarat and western parts of Rajasthan, India (Fig. 1). The area has arid to semi-arid climate with average rainfall ranging from 100 mm in the western deserts to 650 mm in the SE (Agrawal et al., 1980; Gupta et al., 1997; GSI, 2011). The area is nearly flat, with imperceptible slopes, except in some regions where residual hills of the Aravalli

Please cite this article in press as: Bharti, R., et al. Spectral pathways for exploration of secondary uranium: An investigation in the desertic tracts of Rajasthan and Gujarat, India. Adv. Space Res. (2015), http://dx.doi.org/10.1016/j.asr.2015.07.015

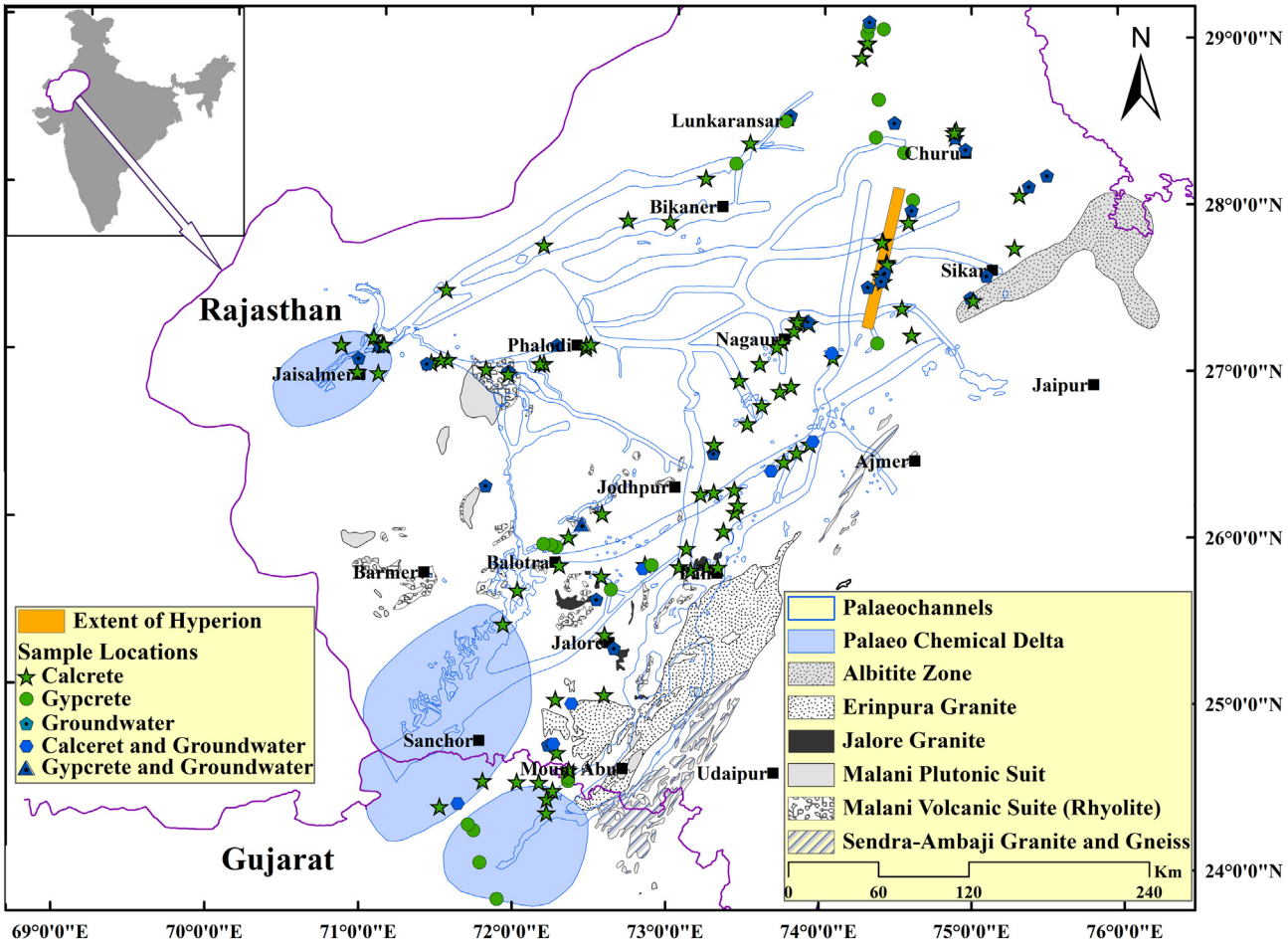

Fig. 1. Map depicting the distribution of source rocks (rich in U, V and K), palaeochannel network, chemical deltas and sites of duricrust and groundwater sampling.

are present. The study area mainly consists of rocks of the Precambrian to the Quaternary periods (Table 1). From the source rock perspectives, the albitite bearing Aravalli Super Group, post Aravalli granitic, rhyolite intrusives, and Delhi Supergroup are very important (Fig. 1). The Fe–Mg rich Erinpura granite contains about 11 ppm of U_3O_8 and 78 ppm of ThO_2 (Maithani et al., 2015) whereas the Jalore granite has an average concentration of 4.8 ppm uranium (Kochhar, 2000). The uranium concentration in Malani plutonic suit range between 8.2 and 18.4 ppm whereas Malani rhyolite have 6.7 ppm (Aqeel and Ali, 2008). The concentration of uranium in Sendra-Ambaji Granite and Gneiss is very high which ranges between 54 and 1696 ppm (Deb et al., 2001). The meta-sediments and meta-basics of the Delhi Supergroup are excellent source rocks for vanadium and related trace elements. Besides these, albitite related uranium mineralization also occurs within the study area (Kochhar, 1989).

From the palaeoclimate perspectives, the study area experienced a warm, humid Neogene period that facilitated extensive weathering and release of solutes (Ca, Mg, U, V and K) from the parent rock (Gupta et al., 1997; Bakliwal and Wadhawan, 2003; Sinha et al., 2004). Since the Pleistocene period, the climate shifted towards semi arid conditions resulting in the sluggish surface and groundwater flow systems. The ongoing arid conditions ever since the Holocene period further accentuated the playa formation and associated evaporite deposits (Sinha et al., 2004; Ramakrishnan and Tiwari, 2006). From exploration perspectives, these fluvial and lacustrine deposits of the Quaternary age are important. Thus, the study area has all the essential conditioning factors to facilitate the enrichment of uranium in secondary environment.

3. Methodology

The methodology adopted in this study (Fig. 2) can be grouped under three broad categories namely (i) satellite data processing and analyses, (ii) field survey and sampling, and (iii) geochemical analyses. Since the target areas are mainly calcretes (rich in Mg-calcites) and gypcrete (rich in gypsum) associated with palaeochannels, emphasis is given to map these duricrusts using satellite data. Though multispectral satellite data can map the calcite and gypsum rich areas, it cannot discern the differences between the calcite and Mg-calcite due to a large spectral bandwidth. As mapping of groundwater calcretes rich in Mg-calcite is an essential aspect of this work, hyperspectral (Hyperion) data

Please cite this article in press as: Bharti, R., et al. Spectral pathways for exploration of secondary uranium: An investigation in the desertic tracts of Rajasthan and Gujarat, India. Adv. Space Res. (2015), http://dx.doi.org/10.1016/j.asr.2015.07.015

Table 1
Generalized stratigraphic sequence of the study area.

Quaternary	Recent	Wind-blown sand
		Younger alluvium
	Sub-recent	Older alluvium
		Shumar gritstone
Cenozoic	Eocene	Bandah limestone
		Khuyala sandstone
	Palaeocene	Sanu sandstone
Unconformity		
	Cretaceous	Abur limestone
		Pariwar sandstone
Unconformity		
Mesozoic	Jurassic	Bedesar sandstone
		Baisakhi shales
		Jaisalmer Limestone
Unconformity		
		Lathi sandstone
Unconformity		
	Permo-Carboniferous	Bap boulder bed
		Bhadura sandstone
Unconformity		
Palaeozoic	Cambrian	Birmania limestone
		Randha sandstone
		Jodhpur sandstone
		Pokran boulder beds
Major unconformity		
	Precambrian	Malani rhyolites and granites

was used to discriminate it from Mg- free calcretes. Once groundwater calcretes and gypcretes were mapped, insitu radiometric surveys were conducted to identify the anomalous zones. Subsequently, duricrust and groundwater samples collected from these zones were analyzed for radioactive and other elements.

3.1. Processing of Hyperion image

The Hyperion sensor on board the EO-1 satellite measures the energies between 0.35 to 2.57 μm wavelength range in 242 contiguous spectral bands with 30 m spatial resolution (Hubbard and Crowley, 2005). Out of 242 bands, calibrated and noise-free 158 spectral bands were corrected for atmospheric effects using Fast Line-of-Sight Atmospheric Analysis of Spectral Hypercubes (FLAASH) algorithm (Adler-Golden et al., 1999). The parameters chosen for atmospheric correction are given in Table 2. O_2 (762.60 nm) and CO_2 (2052.45 nm) absorption wavelengths were used to recalibrate the spectral shifts in both spectrometers. To simulate the atmospheric conditions and estimate the effects of multiple scattering in the data, discrete ordinate (DISORT) method was used. The DISORT algorithm permits fine resolution spectral retrieval and also the efficient and accurate estimate of atmospheric parameters causing multiple scattering (Stamnes et al., 1988; Berk et al., 2002; Perkins et al., 2005, 2012). For the better accuracy in SWIR wavelength region, 1 cm^{-1} Modtran Resolution was used (Adler-Golden et al., 1999). The efficiency of atmospheric correction was estimated by comparing Hyperion and insitu reflectance spectra (San and Suzen, 2010). In this study, insitu spectra collected over a homogenous, flat area like dried playas were correlated with corresponding Hyperion pixel spectra (Fig. 3) and found to have excellent correlation ($R^2 = 0.80$ to 0.96). For reducing the noise and data dimensionality, Minimum Noise Fraction (MNF) (Green et al., 1988) algorithm was used. The noise whitened MNF bands were inverse transformed for matching with the field spectra. Finally, processed Hyperion image was classified using lab-measured spectra of Mg rich calcrete using Spectral Angle Mapper (SAM) technique (Eq. (1); Kruse et al., 1993).

Table 2
FLAASH model parameters used to correct atmospheric effects in the Hyperion data.

Parameters used for atmospheric correction	
Ground elevation	350 m
Atmospheric model	Tropical
Water absorption feature	1135 nm
Aerosol retrieval	2-Band (K–T)
Aerosol model	Rural
Wavelength recalibration	Yes
MODTRAN multiscatter model	DISORT
MODTRAN resolution	1 cm^{-1}

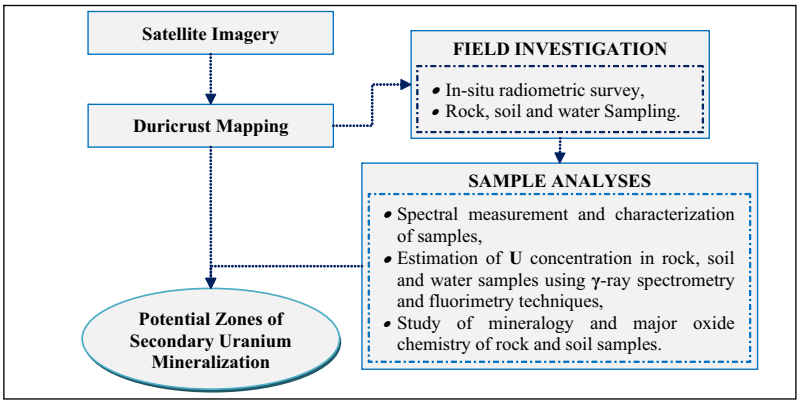

Fig. 2. Work flow depicting the adopted methodology.

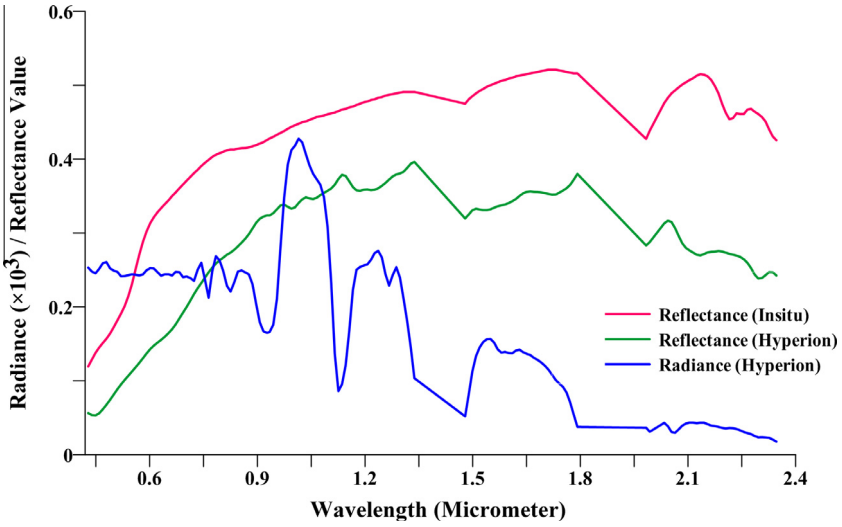

Fig. 3. Comparison of spectral plots illustrating the efficacy of atmospheric correction.

$$\alpha = \cos^{-1}\left[\frac{\sum_{i=1}^{nb} t_i r_i}{\left(\sum_{i=1}^{nb} t_i^2\right)^{1/2}\left(\sum_{i=1}^{nb} r_i^2\right)^{1/2}}\right] \quad (1)$$

where, *nb* is the number of bands, t_i is the target spectrum (image), and r_i is the reference spectrum (library).

3.2. Field investigations

3.2.1. Insitu radiometric analyses

RS-230 BGO Super-SPEC (Radiations Solutions Inc.) γ-ray spectrometer was used for insitu radiometric survey. This instrument is designed for field survey and optimized to provide total count as well as assay values for K (%), U (ppm) and Th (ppm) (Table 3). Before measurement, the spectrometer was calibrated for background concentration. After stabilization of spectrometer, total count mode was used to discover the anomalous zones (>3 Sigma level of the background) and subsequently, concentrations of U, Th and K were measured in assay mode for 600 s (Fig. 4). Since, the source-sensor geometry, detector type and equilibrium of ^{238}U decay series strongly influence the measurement of radio nuclides; the assay values estimated in the field were required to be correlated with conventional geochemical analyses for accuracy.

3.2.2. Duricrust and water sampling

Calcrete and gypcrete samples were collected from the anomalous areas (identified through γ-ray spectrometer) for further lab-based analyses. Since, a thick alluvial cover

Fig. 4. Field photo of calcrete profile with anomalous γ-activity.

can suppress the γ-radiation, groundwater samples were also collected to study the uranium mineralization and mobility of radioactive elements (Cameron et al., 2002; Hou et al., 2007; Noble et al., 2011). For uranium concentration and bulk chemical composition, standard water sampling technique (Tosheva et al., 2004; Waterwatch, 2005; Sundaram et al., 2009) was followed that includes decontamination of sample containers with double distilled water. For uranium analysis, pH of water samples were maintained below 2 using nitric acid to prevent it from biological activities and precipitation (Tosheva et al., 2004; Waterwatch, 2005; Jobbágy et al., 2009; Kumar et al., 2011). To avoid the possibility of oxidation, acidified and

Table 3
Specification of RS-230 BGO Super-SPEC gamma-ray spectrometer.

Model	RS-230	Detector type	Scintillation detector
Detector	Bismuth–Germanium-Oxide (BGO)	Detector size	6.3 cubic inches
Operational temperature	−20 to 50 °C	Output data	1024 channel spectra (30–3000 keV)
Live assay value	K in %; U and Th in ppm		

Please cite this article in press as: Bharti, R., et al. Spectral pathways for exploration of secondary uranium: An investigation in the desertic tracts of Rajasthan and Gujarat, India. Adv. Space Res. (2015), http://dx.doi.org/10.1016/j.asr.2015.07.015

non-acidified sample containers were sealed without any air. During water sampling, insitu pH and Eh values were also measured. Fig. 1 represents the sampling and insitu radiometric survey locations.

3.3. Sample analyses

3.3.1. Radiometric analysis of calcrete and gypcretes

In the process of ^{238}U decay, γ-ray energies are emitted which can be measured by γ-ray spectrometers. In case of secular equilibrium (half life of daughter element is much less than the parent nuclide), measured energies can be used for direct estimation of parent nuclide's concentration (IAEA-TECDOC-1363, 2003; Ebaid, 2010; Tsurikov, 2009; Gilmore, 2011). In this study, estimation of ^{238}U using High Purity Germanium (HPGe) detector in controlled environment and standard sample preparation procedure (ASTM, 2010a,b; Gilmore, 2011) were followed. This involves (i) removal of moisture content from the sample, (ii) pulverization (<200 microns grain size) to get homogenous mixture, and (iii) encapsulation of the processed samples in airtight plastic containers (predefined geometry–7 cm × 8 cm) for about 10 half-lives of ^{222}Rn (i.e. about 30 days). Activity of the reference standard (known), background (B) and samples (S) were measured for about 60,000 s (T). Subsequently, the activity of uranium and thorium in calcrete and gypcrete samples was estimated using Eq. (2)(IAEA-TECDOC-1363, 2003; Gilmore, 2011).

$$Activity\ (Bq/kg) = \frac{N \times 100 \times 100}{T \times \gamma \times \eta \times W} \quad (2)$$

where, N is the net count (background subtracted), T is the measurement time (s), γ is the γ-ray emission probability (%), η is the relative efficiency (%) for a particular gamma energy, and W is the weight of sample.

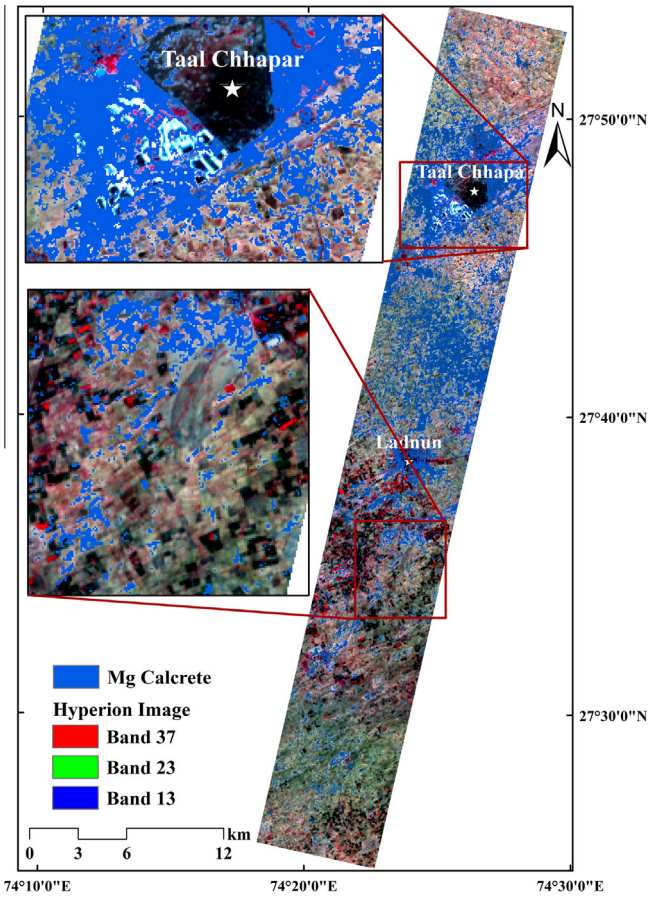

Fig. 6. Distribution of calcretes rich in Mg-calcites mapped using Hyperion image and lab-measured spectra.

3.3.2. Estimation of uranium concentration in water sample

Groundwater samples collected from the field were analyzed for uranium concentration with LED fluorimeter (Quantalase). The spectral absorption due to

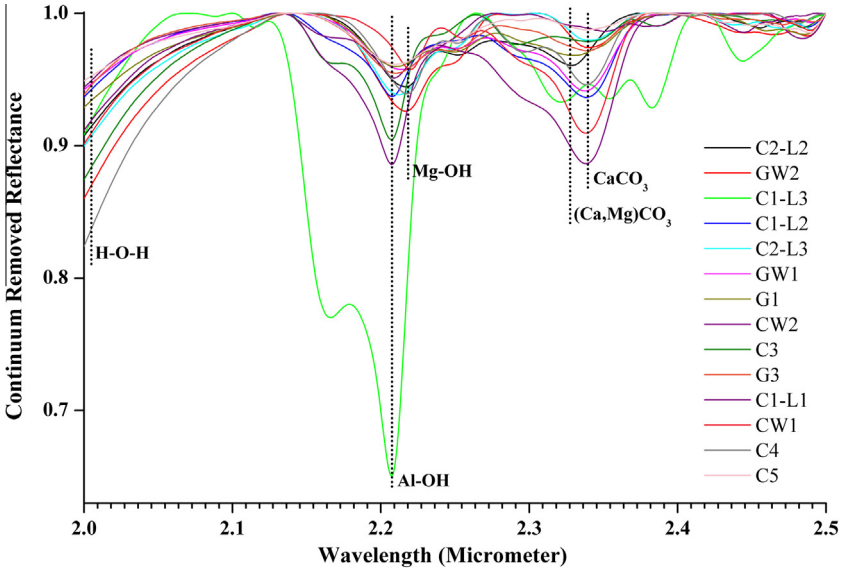

Fig. 5. Reflectance spectra of calcrete samples showing the shift in spectral absorption position due to Mg substitution in calcite.

Please cite this article in press as: Bharti, R., et al. Spectral pathways for exploration of secondary uranium: An investigation in the desertic tracts of Rajasthan and Gujarat, India. Adv. Space Res. (2015), http://dx.doi.org/10.1016/j.asr.2015.07.015

photoluminescence of uranyl ion at 410 nm wavelength was used to estimate the concentration (Veselsky et al., 1988; So and Dong, 2002; Tosheva et al., 2004). The sample preparation for this analysis involved drying of 100 ml of acidified water samples by boiling and then acidifying with 5 ml of nitric acid. Samples were again dried and subsequently diluted to the known volume by adding double distilled water into it. Since, LED fluorimeter has detection limit between 0.1 to 20 μg/l, samples with higher concentration required additional dilution before the actual measurements. In addition to U, groundwater samples were also analyzed for the potassium, vanadium, thorium, phosphate and calcium using Inductively Coupled Plasma - Atomic Emission Spectroscopy (ICP-AES; HORIBA Jobin Yvon-ULTIMA 2).

3.3.3. Estimation of Uranyl compound Solubility Index

Results of hydrogeochemical analyses have been successfully used for the investigation of secondary enrichment of uranium (Bowell et al., 2008; Noble et al., 2011). Based on the dissolution of carnotite (Eq. (3)), Mann and Deutscher (1978) have proposed the Solubility Index (SI), which was further modified by Middleton (1984), (Eq. (4)) to evaluate the equilibrium status between the groundwater and carnotite precipitation for practical applications. The SI model requires input for uranium and vanadium in μg/l, and potassium and bi-carbonate in mg/l. If the SI value is zero, system will be in equilibrium whereas, positive value indicates oversaturation and negative value indicates the dissolution of carnotite. Based on field observations, Middleton (1984) and Noble et al. (2011) suggested that the SI values ranging between −3 and 0 are strongly indicative of potential zones of carnotite occurrence. Thus, for regional scale exploration, the SI is very effective in delineating the anomalous zones (Middleton, 1984).

$$\frac{1}{2}K_2(UO_2)_2.V_2O_8.3H_2O + 2H^+ \rightarrow K^+ + UO_2^{+2} + H_2VO_4^- \quad (3)$$

$$SI = \log\frac{[U][V][K]}{1.13 \times 10^4[HCO_3]^2} \quad (4)$$

3.3.4. Reflectance spectral measurement and preprocessing

Fieldspec®3 (ASD Inc.), a portable field spectroradiometer has been used to measure the reflectance spectra between 0.3 and 2.5 μm range. Since the spectra are influenced by source-sensor geometry, field of view, roughness and anisotropy of the sample, a standard procedure addressing above parameters was followed for calibration and spectral acquisition (Salisbury, 1998; Bharti et al.,

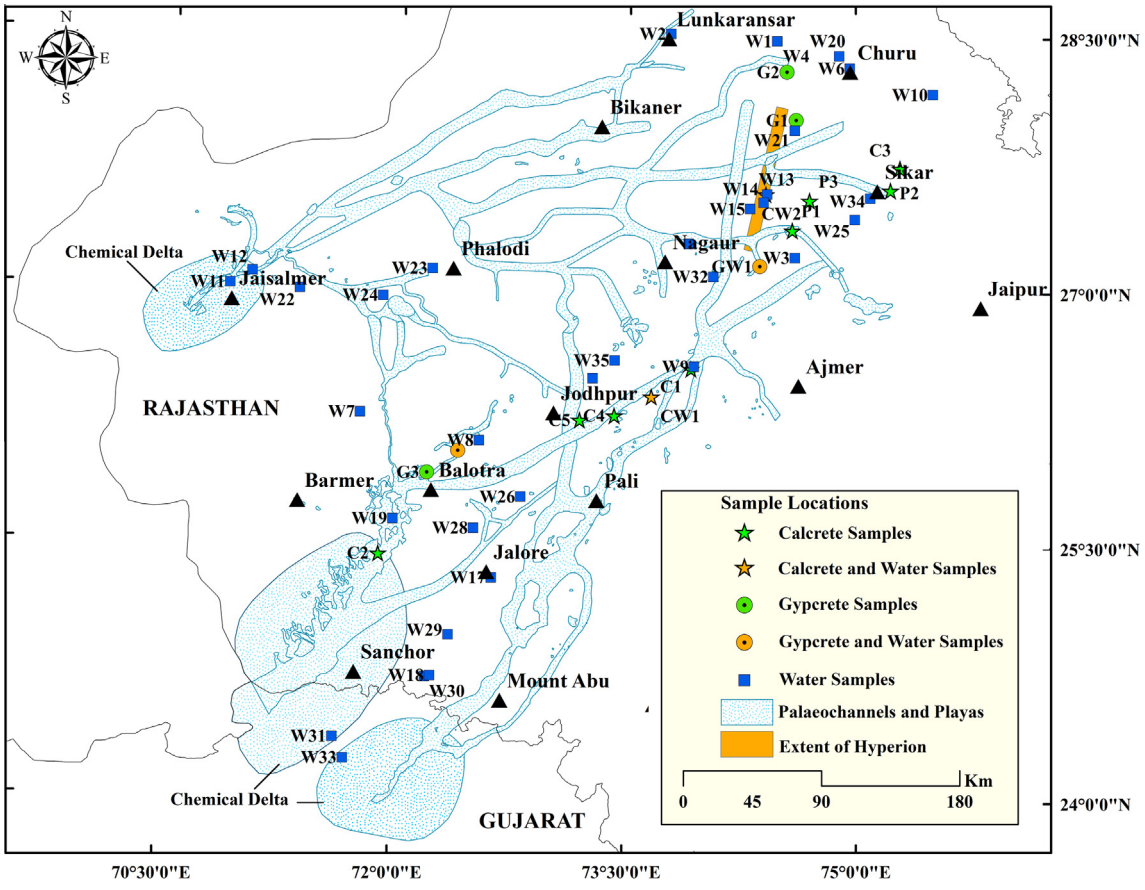

Fig. 7. Field locations of representative samples selected for analyses.

2012). To stabilize internal noises and detectors, Fieldspec®3, was kept running for 2 h and subsequently calibrated for internal instrument noises (Dark Current) and down welling radiances (Lambertian Surface: White Reference). Due to molecular vibration, water has overtone absorption features at 1.4 μm and 1.9 μm (Clark, 1999). In this study, the spectral noises caused by water vapor absorptions were corrected from the measured spectra using the procedures of Kusuma et al. (2010) and resampled them to Hyperion bandwidth (Bharti and Ramakrishnan, 2014). Field samples were also analyzed for the mineralogy (semi-quantitative) and major oxide chemistry using XRD (PANAlytical- X'Pert PRO) and XRF (PANAlytical- PW2404) respectively.

4. Results

4.1. Spectroscopy and distribution of duricrusts

Calcite (28–64%), quartz (9–55%), feldspar (12–30%) and pyroxene (12–41%) with minor amounts of clay minerals are found to be the predominant mineralogy of calcretes. The major oxide chemistry of these calcretes include CaO (46.7–84.5%), SiO_2 (8.4–41.1%), Fe_2O_3 (0.3–2.9%), MgO (0.1–3.4%) and Al_2O_3 (1.2–6.6%). In the measured spectra of calcrete samples, 2.30–2.35 μm absorption bands are prominent (Fig. 5). Depending upon the carbonate content in the sample and level of signal to background noise (SNR), other weak absorption features may not be apparent. From the reflectance spectra of calcretes it is observed that increase in Mg content results in shifting of 2.35 μm absorption feature towards shorter wavelength region (i.e. 2.30 μm), (Clark, 1999). Fig. 6 represents the spatial distribution of Mg rich calcretes (3.4%), mapped from Hyperion image and lab measured spectra using SAM technique. Based on confusion matrix, the estimated classification accuracy is 72.15%.

4.2. Mineralogy, geochemistry, and radioactivity

Based on the distribution of Mg calcretes deciphered from Hyperion image, 160 locations along palaeochannels and playas were visited to measure the radioactivity. From these locations, 42 groundwater and 18 duricrust representative samples were collected for detailed analyses (Fig. 7). It is evident from the XRD results that the calcretes contain mostly calcite (40–60%), quartz (30–45%) and feldspars (10–15%) with minor proportions of pyroxene, amphibole, mica and clay minerals. The average values of major oxides found in calcretes are CaO (33%), SiO_2 (43%), Al_2O_3 (14%), Fe_2O_3 (4%), MgO (4%), K_2O (2%) and Na_2O_3 (0.5%). In case of gypcretes, gypsum is the predominant mineral (25–40%) with good proportions of dolomite (28–33%), quartz (10–15%) and albite (23–36%). The major oxide chemistry of gypcrete includes CaO (18%), SiO_2 (58%), Al_2O_3 (10%), Fe_2O_3 (4%), MgO (8%), K_2O (2%) and Na_2O_3 (1%).

Table 4
Mineralogy and major oxide chemistry of the representative field samples.

Location details		HPGe (Bq/kg) Lab measurement			BGO (Bq/kg) In-situ measurement			Major oxide geochemistry (Wt.%)							
Id	Name	U	Th	K	U	Th	K (%)	CaO	Fe_2O_3	K_2O	MgO	P_2O_5	SiO_2	Al_2O_3	Na_2O_3
C1	Indawar L1	27.3	55.0	327.0	27.2	5.7	11.8	4.8	9.5	3.0	3.3	0.10	48.3	30.3	0.6
	Indawar L2	11.0	16.3	205.0	27.2	3.7	17.7	50.4	1.9	1.4	1.1	0.00	38.5	6.5	0.3
	Indawar L3	33.0	91.0	133.0	98.8	124.8	8.0	15.4	4.0	0.7	0.8	0.00	48.1	30.9	0.2
C2	Paylan Kalan L2	39.5	20.0	135.0	44.4	52.4	1.5	14.1	4.6	1.7	18.0	0.00	50.1	11.0	0.4
	Paylan Kalan L3	14.5	24.3	253.0	44.4	52.4	1.5	21.5	5.2	2.0	4.3	0.10	54.2	12.4	0.3
C3	Khirod	31.0	87.0	760.0	18.5	14.6	12.0	31.1	6.5	3.1	2.1	0.00	43.3	13.7	0.2
C4	Kaparda	19.3	19.0	80.0	46.9	–	–	47.5	2.8	0.5	2.9	0.04	38.4	6.8	1.1
C5	Jodhpur to Dangiyawas	15.3	29.0	334.0	43.2	–	–	4.7	5.7	3.8	2.9	0.07	63.3	18.3	1.2
CW2	Dujar	11.3	18.3	45.0	11.4	61.0	0.5	74.4	0.7	0.5	1.3	0.02	18.5	4.4	0.2
CW1	Malawas	23.0	24.3	260.0	43.2	142.3	2.0	66.6	0.8	1.4	1.5	0.04	25.0	4.4	0.4
G1	Ratangarh	19.0	35.0	322.0	49.4	56.9	2.1	26.7	4.2	1.8	13.8	0.10	45.0	7.8	0.6
G2	Ranasar Beekan	34.0	21.5	286.0	61.7	81.3	2.0	36.8	3.1	1.3	13.0	0.10	39.0	6.0	0.8
G3	Sambhra Playa	25.3	45.3	290.0	19.7	41.5	17.0	5.4	5.7	2.3	4.0	0.20	68.8	12.9	0.8
GW1	Khatu Khurd	21.0	32.6	206.0	61.7	–	–	3.1	2.4	0.4	2.6	0.04	82.9	8.0	0.6
GW2	Thob	53.6	41.6	329.0	49.4	63.41	18.0	16.6	6.1	2.1	8.5	0.20	52.9	13.0	0.7
P1	Didwana	2345.7	–	–	–	–	–	–	–	–	–	–	–	–	–
P2	Charan Ka Bas	611.1	–	–	–	–	–	–	–	–	–	–	–	–	–
P3	Lachhiri	166.7	–	–	–	–	–	–	–	–	–	–	–	–	–

C-calcrete, G-gypcrete, CW-calcrete and water, GW-gypcrete and water, P-Published high and U-calcrete locations.

Table 4 represents the concentration of radionuclides (U, Th and K) measured with BGO (in field) and HPGe (in laboratory condition) with their major oxide chemistry. The values of uranium, thorium and potassium measured in the field (BGO) ranges from 11.1–98.7 Bq/kg, 3.6–142.3 Bq/kg and 0.5–18.0% respectively. Whereas, the values measured in lab for the same sequence with HPGe ranges from 9.8–53.1 Bq/kg, 16.3–91.1 Bq/kg, and 45–760 Bq/kg respectively. Compared to lab measurements, insitu values are relatively high. Misra et al. (2011) and Ramesh Kumar et al. (2011) have reported significantly higher uranium concentration in calcrete samples ranging from 166.7 Bq/kg to 2345.7 Bq/kg from deep borehole samples in this area. Measured concentrations of U, Th and K correlate well among themselves ($R^2 = 0.80$ to 0.84). However, among the measured major oxides, uranium has good positive correlation only with MgO ($R^2 = 0.71$). The uranium concentration in water samples is observed to vary between 0.2 and 1791.7 μg/l (Table 5). From the spatial distribution of anomalous concentrations (20.0–1791.7 μg/l) it is evident that such zones are typically located very close to the confluence of palaeochannels and chemical deltas located near Bhukhan, Sev Ki Kalan, Aampura, Tharad, Kotharwada and Matasukh (Fig. 8; Table 6).

From the Solubility Index perspectives, concentration of Ca, K, and V range from 12.5 to 203.0 mg/l, 1.2 to 99.3 mg/l, and 0.14 to 62.18 mg/l respectively. Similarly,

Table 5
Fluorimetry and geochemical analyses results of water samples.

Sample details		Fluorimetry	ICP-AES (in (mg/l))				
Id	Location name	U (μg/l)	Ca	K	P	Th	V
W1	Sardarshahar	12.2 ± 0.9	–	–	–	–	–
W2	Lunkaransar	4.1 ± 0.6	–	–	–	–	–
W3	Aajdoli	112.8 ± 2.9	76.96	5.52	0	0.01	0.03
W4	Haryasar	21.9 ± 3.1	–	–	–	–	–
W5	Mankeria	18.8 ± 1.2	–	–	–	–	–
W6	Churu	42.7 ± 2.2	–	–	–	–	–
W7	Dandalwas	7.8 ± 0.7	53.03	3.06	0.20	0.00	0.06
W8	Deriya	45.9 ± 2.9	177.58	8.98	0.28	0.00	0.02
W9	Indawar	0.8 ± 0.3	177.51	1.65	0.00	0.00	0.01
W10	Bagar	7.2 ± 1.6	41.80	1.46	0.17	0.00	0.01
W11	Dadawadi Temple	0.2 ± 0.1	–	–	–	–	–
W12	Hadda Village	2.0 ± 0.5	–	–	–	–	–
W13	Ladnun to Didwana	16.7 ± 1.8	–	–	–	–	–
W14	Ber Village	11.5 ± 0.7	–	–	–	–	–
W14	Ber Village	11.0 ± 1.9	–	–	–	–	–
W15	Jhardiya	7.2 ± 0.8	–	–	–	–	–
W16	Kishanpura	12.2 ± 1.3	–	–	–	–	–
W17	Jalore	81.9 ± 20.3	94.99	1.44	0.00	0.00	2.81
W18	Doongri	1.5 ± 0.3	46.03	1.83	0.03	0.00	0.01
W19	Bhukan-1	20.0 ± 4.9	–	–	–	–	–
W19	Bhukan-2	38.3 ± 3.9	177.12	99.32	0.34	0.01	0.00
W20	Somaser	20.7 ± 1.8	–	–	–	–	–
W21	Parihara	13.8 ± 1.6	–	–	–	–	–
W22	Chandan	18.8 ± 1.7	–	–	–	–	–
W23	Bengti Kalan and Kundal	2.1 ± 0.4	–	–	–	–	–
W24	Near Gomat	12.4 ± 1.0	–	–	–	–	–
W25	Rajpura	10.8 ± 0.6	22.00	2.24	0.10	0.00	0.02
W26	Gelawas	503.0 ± 61.4	167.76	20.94	2.53	0.00	28.17
W27	Sev ki Galan	445.0 ± 41.1	17.60	4.35	0.00	0.00	62.18
W28	Mokalsar	3.9 ± 0.5	26.14	2.05	0.00	0.00	0.00
W29	Munthala Kaba-1	216.8 ± 35.6	76.72	2.17	0.00	1.12	8.28
W29	Munthala Kaba-2	401.6 ± 52.8	172.81	3.22	0.00	0.00	8.16
W30	Aampura	50.1 ± 15.9	62.97	5.43	0.00	0.00	2.37
W31	Tharad	1508.2 ± 126.9	91.46	5.13	0.00	0.16	16.98
W32	Matasukh	1791.7 ± 159.6	203.30	7.30	0.00	34.30	0.00
W33	Kotarwada	920 ± 56.2	12.53	1.24	0.34	0.02	0.03
W34	Sikhar	0.5 ± 0.1	28.91	1.54	0.69	0.01	0.01
W35	Sopra Village	5.5 ± 0.5	51.25	2.29	0.38	0.00	0.00
GW1	Khatu Khurd	10.2 ± 0.9	19.22	9.34	2.27	0.01	0.14
GW2	Thob Gypsum Mine	71.9 ± 5.8	146.27	9.17	0.00	0.01	0.00
CW1	Malawas	6.8 ± 0.7	31.39	6.44	0.55	0.01	0.00
CW2	Dujar Village	21.9 ± 1.9	–	–	–	–	–

W-Water, CW-calcrete and water, and GW-gypcrete and water sample locations.

Please cite this article in press as: Bharti, R., et al. Spectral pathways for exploration of secondary uranium: An investigation in the desertic tracts of Rajasthan and Gujarat, India. Adv. Space Res. (2015), http://dx.doi.org/10.1016/j.asr.2015.07.015

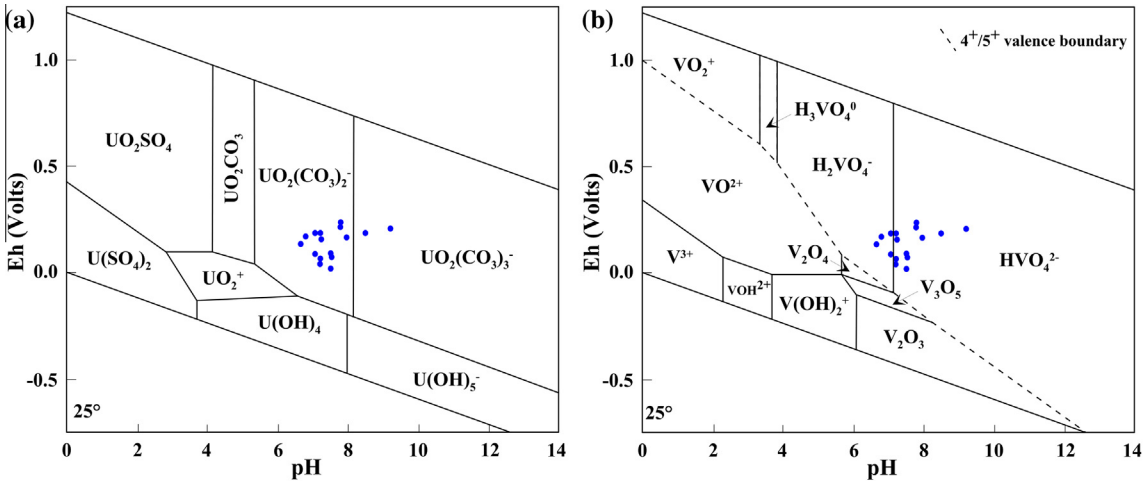

Fig. 8. Eh–pH plots of representative groundwater samples showing (a) the valence states of the uranium in groundwater samples and (b) species and valence state of vanadium.

Table 6
Representing the concentration of essential components of carnotite and Solubility Index (SI) for the secondary uranium mineralization.

Id	Location name	U (μg/l)	K (mg/l)	P (mg/l)	V (μg/l)	HCO_3 (mg/l)	SI
W30	Aampura	50.1	5.43	0.0	2370.0	405.0	−3.46
W3	Aajdoli	112.8	5.52	0.0	30.0	560.0	−5.28
W17	Jalore	81.9	1.44	0.0	2810.0	590.0	−4.07
W29	Munthala Kaba-1	216.8	2.17	0.0	8280.0	780.0	−3.25
W31	Tharad	1508.2	5.13	0.0	16980.0	1225.0	−2.11
W27	Sev Ki Galan	445	4.35	0.0	62180.0	1950.0	−2.55
W18	Doongri	1.5	1.83	0.03	10.0	285.0	−7.52
W25	Rajpura	10.8	2.24	0.1	20.0	355.0	−6.47
W10	Bagar	7.2	1.46	0.17	10.0	285.0	−6.94
W7	Dandalwas	7.8	3.06	0.2	60.0	265.0	−5.74
W8	Deriya	45.9	8.98	0.28	20.0	575.0	−5.66
W33	Kotarwada	920	1.24	0.34	30.0	630.0	−5.12
W26	Gelawas	503	20.94	2.53	28170.0	590.0	−1.12
W29	Munthala Kaba-2	401.6	3.22	0.0	8160.0	145.0	−1.35

concentration of anions such as HCO_3, SO_4 and P range from 405.0 to 1950.0 mg/l, 0 to 2.53 mg/l, and 16.5 to 266.3 mg/l respectively. In groundwater, concentration of Th is observed to be less than 0.2 mg/l (Table 5). The measured Eh and pH values during sampling vary between 55–209 mV and 6.6–9.16 respectively. Uranium in groundwater samples shows strong correlation with HCO_3 ($R^2 = 0.80$). However, the relationship between Eh and U in groundwater is highly correlated only when the U concentrations are relatively higher ($U > 20$ μg/l).

5. Discussion and conclusions

Massive deposits of secondary uranium have been reported from duricrusts of Australia, Namibia and Chile. Availability of source rocks (rich in Ca, Mg, U, V and K), palaeochannel networks, present and palaeoclimatic conditions with suitable Eh and pH conditions play very important role in such mineralization in calcretes and gypcretes (Butt et al., 1977; Carlisle, 1983; Arakel, 1988; Cameron et al., 2002; Bowell et al., 2009). In the investigated area, source rocks of U, V and K such as Albitite Zone, Erinpura-, Malani-, and Jalore-granite (Fig. 1) are abundant (Kochhar, 1989; GSI, 1999). In addition to this, palaeoclimate favored intense weathering (Sinha et al., 2004; Ramakrishnan and Tiwari, 2006) of the above mentioned source rocks and availability of well-knitted palaeochannel systems (Bajpai, 2004; Jain et al., 2004) to carry the U, V and K, supported the secondary uranium enrichments (Fig. 7). The study area thereby satisfies all necessary conditions for secondary uranium enrichment in duricrusts associated with chemical deltas and palaeochannels. Thus mapping the distribution of calcrete and gypcrete along the palaeochannels is an important component of exploring such deposits.

Though U has characteristic spectral absorption features in the visible region, it is often difficult to identify its presence based on this due to low concentration (usually in ppm). For this purpose, the Mg-calcretes, which are precipitated from groundwater, were used as a proxy to explore secondary uranium enrichments. In this study, the prominent Mg-calcite absorption features (Fig. 5)

Please cite this article in press as: Bharti, R., et al. Spectral pathways for exploration of secondary uranium: An investigation in the desertic tracts of Rajasthan and Gujarat, India. Adv. Space Res. (2015), http://dx.doi.org/10.1016/j.asr.2015.07.015

between 2.30 μm and 2.35 μm wavelength region was used to map the groundwater calcrete using Hyperion data. As the Mg content increases in the calcrete, 2.35 μm absorption feature shifts to 2.30 μm wavelength region (Hunt and Salisbury, 1970; Clark, 1999; Christensen et al., 2000; Van-der-meer, 2004; Bharti and Ramakrishnan, 2014). Based on this fact, representative lab-measured spectra of Mg-calcrete, processed Hyperion data and SAM technique were used to map the spatial distribution (Fig. 6) with 72.15% overall accuracy.

Uranium concentration measured through HPGe (laboratory) in duricrusts, indicates that the Sambhra Playa, Indawar, Khirod, Ranasar Beekan, Paylan Kalan, Thob, Lachhiri, Charan Ka Bas and Didwana have high uranium and thorium concentrations (Table 4). A few more locations such as Jodhpur to Dangiyawas, Kaparda, Ratangarh and Khatu Khurd were also observed to show anomalous concentration through insitu radiometric survey. Due to active dune activity and thick cover of alluvium, γ-radiation is often suppressed and many places remained unexplored. In such cases, groundwater analysis is considered the best alternative to find the anomalies (Noble et al., 2011). The groundwater samples collected (Table 5) from locations such as Dujar, Bhukhan, Churu, Deriya, Aampura, Thob, Jalore, Haryasar, Aajdoli, Munthala Kaba, Sev Ki Kalan, Gelawas, Kotarwada, Tharad and Matasukh (Fig. 7) show very high concentration of uranium (21.9–1791.7 μg/l). These values are higher than the concentrations (1–700 μg/l, with 14 μg/l mean value) found in the Northern Yilgarn deposit (Noble et al., 2011). In particular, such anomalous zones are found either close to the junctions of palaeochannels or within the chemical deltas (Fig. 7).

One of the important components necessary during the secondary enrichment of uranium as carnotite in calcretes and gypcretes is the availability of vanadium in groundwater. Concentrations of V found in the groundwater samples collected from Aampura, Jalore, Munthala Kaba, Tharad, Gelawas, and Sev Ki Kalan indicate a reasonably high range from 0.14 to 62.18 mg/l (Table 6). The next essential component of carnotite is potassium which is found in the samples of Dandalwas, Munthala Kaba, Sev ki Kalan, Tharad, Aampura, Aajdoli, Malawas, Matasukh, Deriya, Thob, Khatu Khurd, Gelawas, Bhukhan ranging from (3.1–99.3 mg/l). Compared to these results, vanadium concentration found in groundwater samples of Northern Yilgarn deposit is much less (<251 μg/l) whereas the reported mean concentration of potassium (32 mg/l) is relatively more (Noble et al., 2011). Calcium is abundant in all samples whereas phosphate is found in limited samples.

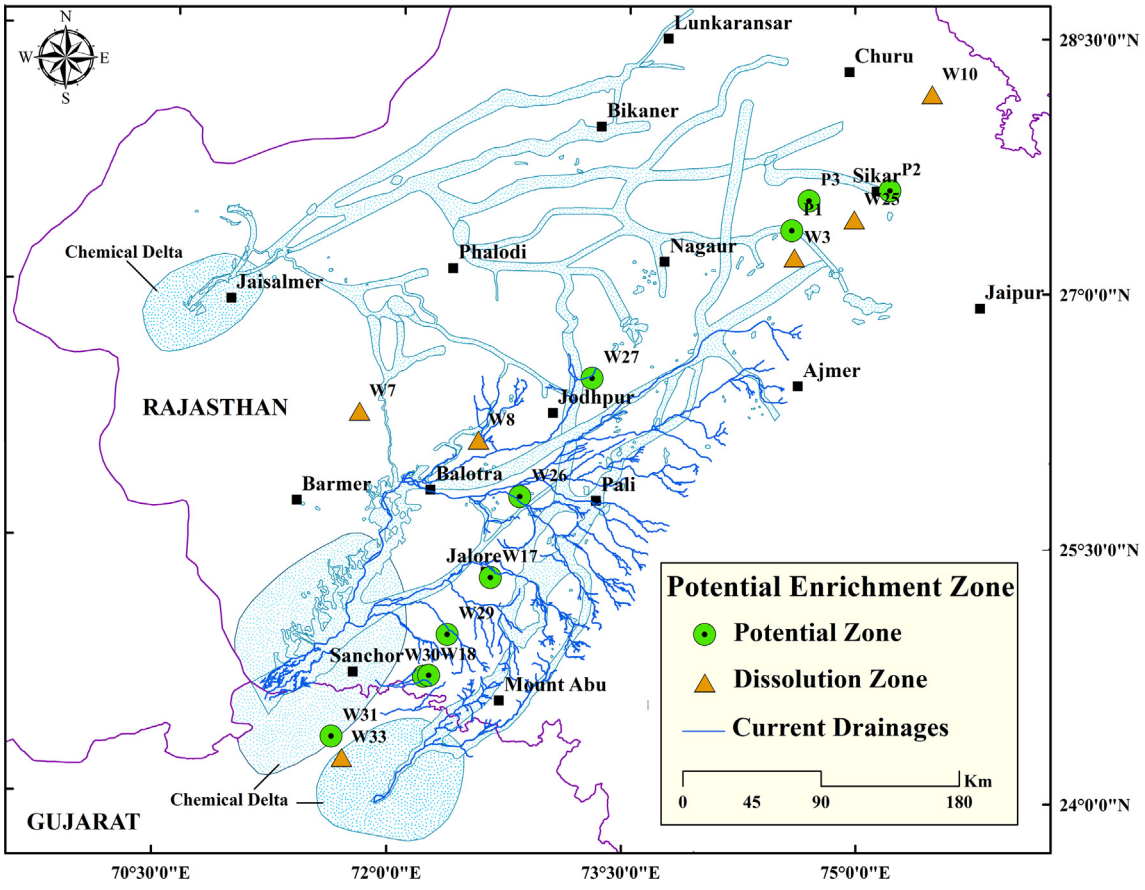

Fig. 9. Map indicating the potential enrichment zones for secondary uranium.

Please cite this article in press as: Bharti, R., et al. Spectral pathways for exploration of secondary uranium: An investigation in the desertic tracts of Rajasthan and Gujarat, India. Adv. Space Res. (2015), http://dx.doi.org/10.1016/j.asr.2015.07.015

In addition to the availability of above mentioned essential elements in groundwater, the Eh and pH is also very important in the uranyl compound speciation and precipitation (Carlisle, 1983; Arakel, 1988; Bowell et al., 2008; Hou et al., 2007; Noble et al., 2011). The mobility of uranium is strongly influenced by oxidation state and available ligands such as carbonate, phosphate and hydroxyl complexes (Bastrakov et al., 2010). In case of highly alkaline fluids, solubility of uranium depends on pH as well as oxidation states (Carlisle, 1983; Arakel, 1988; Bowell et al., 2008; Hou et al., 2007; Bastrakov et al., 2010; Noble et al., 2011). The measured Eh and pH values for the collected samples are used to identify the dominant chemical species of uranium and vanadium. It is evident from the Fig. 8(a) and (b) that $UO_2(CO_3)_2^-$, $UO_2(CO_3)_3^-$, HVO_4^{2-} and $H_2VO_4^-$ are the dominating species in groundwater samples of the investigated area. Uranium and vanadium are expected to be present in the form of dissolved U^{+6} and V^{+5} respectively (Fig. 8(a) and (b)) which are required for the carnotite precipitation. It is evident from the results of geochemical analyses that except locations such as Aampura, Thob, Gelawas, Jalore, Aajdoli, Munthala Kaba, Sev Ki Kalan, Tharad and Matasukh, all other locations have phosphates which could be a reason for the mobility of uranium in groundwater (Table 5). On the basis of SI, Aampura, Jalore, Gelawas, Munthala Kaba, Sev Ki Kalan and Tharad have been identified as the potential zones of uranium enrichment (Table 6; Fig. 9). In addition to this, presence of phosphate in the samples and its role in the mobility of uranium in groundwater is also considered while identifying the potential zones of enrichment. The potential sources of U, V and K are mainly the meta-volcanic rocks of albitites, Erinpura granites, metasediments and a host of igneous intrusives belonging to Delhi Supergroup of rocks.

To sum-up, this work mainly showcases the potential of adopted methodology involving HRS, γ-ray spectrometry, fluorimetry and hydrogeochemistry techniques in exploration of secondary uranium enrichment in the palaeo river valleys and associated sediments. Following are the major conclusions emerging from this study:

- Hyperion data and lab-measured spectra together can map the minor variation in chemical composition efficiently. This is very vital in delineating the calcretes bearing high Mg-calcites that are proven to contain anomalous U, Th and K concentrations.
- Based on the groundwater chemistry and SI, the confluence of palaeochannels and the deltas have been identified as potential zones of carnotite enrichment and hence, the prospective targets for further exploration.
- Based on this investigation and the preliminary results published by Misra et al. (2011), it is evident that the investigated area has very high potential for secondary enrichment of fissile material and field exploration like drilling, γ-ray logging and assaying is necessary to assess the economic viability of such deposits.

Acknowledgement

This research (12ISROC006) was financially supported by Indian Space Research Organization (ISRO), Government of India. Authors thank the United States Geological Survey (USGS) for Hyperion data. Health Physics Division, Bhabha Atomic Research Centre, Mumbai, India is also acknowledged for radiometric and fluorimetric analyses of field samples.

References

Adler-Golden, S.M., Matthew, M.W., Bernstein, L.S., Levine, R.Y., Berk, A., Richtsmeier, S.C., Acharya, P.K., Anderson, G.P., Felde, G., Gardner, J., Hoke, M., Jeong, L.S., Pukall, B., Ratkowski, A., Burke, H.H., 1999. Atmospheric correction for short-wave spectral imagery based on MODTRAN4. Proc. SPIE 3753, 61–69.

Agrawal, D.P., Datta, P.S., Hussain, Z., Krishnamurthy, R.V., Misra, V.N., Rajaguru, S.N., Thomas, P.K., 1980. Palaeoclimate, stratigraphy and prehistory in north and west Rajasthan. Proc. Acad. Sci.-Earth Planet. Sci. 89 (1), 51–66.

Aqeel, A.S., Ali, M., 2008. Evaluation of uranium source potential of Nagar Parkar granites and associated felsic rocks. Internal documents, REOK Pakistan Atomic Energy Commission.

Arakel, A.V., 1988. Carnotite mineralization in inland drainage areas of Australia. Ore Geol. Rev. 3 (1–3), 289–311.

ASTM, 2010. C998–05, Standard Practice for Sampling Surface Soil for Radionuclides. ASTM International, United States, pp. 1–4.

ASTM, 2010. C999–05, Standard Practice for Soil Sample Preparation for the Determination of Radionuclides. ASTM International, United States, pp. 1–3.

Bajpai, V.N., 2004. Hydrogeological evolution of the Luni river basin, Rajasthan, western India: a review. Proc. Acad. Sci.-Earth Planet. Sci. 113 (3), 427–451.

Bakliwal, P.C., Wadhawan, S.K., 2003. Geological evolution of Thar Desert in India-issues and prospects. Proc. Indian Natl. Sci. Acad. Part A 69 (2), 151–165.

Bastrakov, E.N., Jaireth, S., Mernagh, T.P., 2010. Solubility of uranium in hydrothermal fluids at 25–300 °C. Implications for the formation of uranium deposits. Geosci. Aust. Rec. 2010 (29), 91.

Bates, J.L., 1965. Visible and infrared absorption spectra of uranium dioxide. Nucl. Sci. Eng. 21, 26–29.

Berk, A., Adler-Golden, S.M., Ratkowski, A.J., Felde, G.W., Anderson, G.P., Hoke, M.L., Cooley, T., Chetwynd, J.H., Gardner, J.A., Matthew, M.W., Bernstein, L.S., Acharya, P.K., Miller, D., Lewis, P., 2002. Exploiting MODTRAN radiation transport for atmospheric correction: the FLAASH algorithm. In: Proceedings of the Fifth International Conference on Information Fusion, vol. 2, pp. 798–803.

Bharti, R., Ramakrishnan, D., 2014. Uraniferous calcrete mapping using hyperspectral remote sensing. In: IEEE International Geoscience and Remote Sensing Symposium (IGARSS), 13th–18th July 2014, pp. 2902–2905.

Bharti, R., Ramakrishnan, D., Singh, K.D., Nithya, M., 2012. Relevance of mineral texture on bidirectional reflectance and emission spectroscopy: implications for geological remote sensing. In: IEEE International Geoscience and Remote Sensing Symposium (IGARSS), pp. 3046–3049.

Bowell, R.J., Booysens, M., Pedley, A., Church, J., Moran, A., 2008. Characterization of carnotite uranium deposit in calcrete channels, Trekkopje, Namibia. In: Proceedings of Africa Uncovered: Mineral Resources for the future, SEG-GSSA Conference, 7th–10th July 2008, pp. 114–121.

Bowell, R .J., Barnes, A., Grogan, J., Dey, M., 2009. Geochemical controls on uranium precipitation in calcrete palaeochannel deposits of Namibia. In: Proceedings of 24th International symposium of Applied

Geochemistry, Fredericton, New Brunswick, Canada, 1st–4th June 2009, pp. 1–4.

Bryant, R.G., 1996. Validated linear mixture modelling of Landsat TM data for mapping evaporite minerals on a playa surface: methods and applications. Int. J. Remote Sens. 17 (2), 315–330.

Burns, R., 1970. Mineralogical Applications of Crystal Field Theory. Cambridge University Press, Cambridge, 551 p.

Butt, C.R.M., Mann, A.W., 1984. Surficial uranium deposits in Australia: surficial uranium deposits. Report of the Working Group on Uranium Geology Organized by the International Atomic Energy Agency, Vienna, IAEA-TECDOC-322.

Butt, C.R.M., Horwitz, R.C., Mann, A.W., 1977. Uranium occurrences in calcretes and associated sediments in Western Australia. CSIRO, Division of Mineralogy Report, FP16, pp. 1–66.

Cameron, E.M., Leybourne, M.I., Kelley, D.L., 2002. Exploring for deeply covered mineral deposits: formation of geochemical anomalies at the Spence copper porphyry deposit, Chile. Geology 30, 1007–1010.

Carlisle, D., 1978. The distribution of calcretes and gypcretes in the southwestern United states and their uranium favourability. Grand Junction, Dept. Energy Report, GJBX-29-78, 274 p.

Carlisle, D., 1983. Concentration of uranium and vanadium in calcretes and gypcretes. Geological Society, London. Special Publications. vol. 11, pp. 185–195.

Christensen, P.R., Bandfield, J.L., Hamilton, V.E., Howard, D.A., Lane, M.D., Piatek, J.L., Ruff, S.W., Stefanov, W.L., 2000. A thermal emission spectral library of rock-forming minerals. J. Geophys. Res. (Planets) 105 (E4), 9735–9739.

Clark, R.N., 1999. Spectroscopy of rocks and minerals, and principles of spectroscopy. In: Renez, A.N. (Ed.), Manual of Remote Sensing, Remote sensing for the Earth Sciences, vol. 3. John Wiley and Sons, New York, pp. 3–58.

Crosta, A., Mc.Moore, J.M., 1989. Enhancement of Landsat Thematic Mapper imagery for residual soil mapping in SW Minais Gerais State, Brazil: a prospecting case history in Greenstone belt terrain. In: International Proceedings of the Seventh Erim Thematic Conference: Remote Sensing for Exploration Geology, Calgary, Alberta, Canada, 2–6 October, pp. 1173–1187.

Crowley, J.K., 1993. Mapping playa evaporite minerals with AVIRIS data: a first report from death valley, California. Remote Sens. Environ. 44 (2–3), 337–356.

Deb, M., Thorpe, R.I., Krstic, D., Corfu, F., Davis, D.W., 2001. Zircon U–Pb and galena Pb isotope evidence for an approximate 1.0 Ga terrane constituting the western margin of the Aravalli-Delhi orogenic belt, northwestern India.

Ebaid, Y.Y., 2010. Use of gamma-ray spectrometry for uranium isotopic analysis in environmental samples. Rom. J. Phys. 55 (1–2), 69–74.

Gaffey, S.J., McFadden, L.A., Nash, D., Pieters, C.M., 1993. Ultraviolet, visible and near infrared reflectance spectroscopy: laboratory spectra of geologic materials. In: Pieters, C.M., Englert, P.A.J. (Eds.), Remote Chemical Analysis: Elemental and Mineralogical Composition. Cambridge university press, Cambridge, pp. 43–78.

Gilmore, G.R., 2011. Practical Gamma-ray Spectrometry,, John Wiley Sons, Ltd, UK, 381 p.

Goetz, A.F.H., Vane, G., Solomon, J.E., Rock, B.N., 1985. Imaging spectrometry for earth remote sensing. Science 228, 1147–1153.

Green, A.A., Berman, M., Switzer, P., Craig, M.D., 1988. A transformation for ordering multispectral data in terms of image quality with implications for noise removal. IEEE Trans. Geosci. Remote Sens. 26, 65–74.

GSI, 1999. Geological and Mineral Map of Rajasthan. Geological Survey of India, Government of India, India.

GSI, 2011. Geology and Mineral Resources of Rajasthan. Geological Survey of India, third revised ed., Miscellaneous Publication, 30(12).

Gupta, R.P., 2003. Remote Sensing Geology, second ed. Springer- Verlag, Berlin, Heidelberg, New York, 1–656.

Gupta, S.N., Arora, Y.K., Mathur, R.K., Iqbaluddin, Prasad, B., Sahai, T.N., Sharma, S.B., 1997. The Precambrian geology of the Aravalli region, southern Rajasthan and northeastern Gujarat. Geol. Surv. India Memoir 123, 1–262.

Hambleton-Jones, B.B., Toen, P.D., 1978. The geology and geochemistry of calcrete/gypcrete uranium deposits in duricrust, Namib desert, South West Africa. Econ. Geol. 73, 1407–1408.

Hartleb, J.W.O., 1988. The langer Heinrich uranium deposit: Southwest Namibia. Ore Geol. Rev. 3, 277–287.

Heath, A.G., Deutscher, R.L., Butt, C.R.M., 1984. Lake Austin uranium deposit, Western Australia: surficial uranium deposits. Report of the Working Group on Uranium Geology Organized by the International Atomic Energy Agency, Vienna, IAEA-TECDOC-322.

Hou, B., Fabris, A.J., Keeling, J.L., Fairclough, M.C., 2007. Cainozoic palaeochannels hosted uranium and current exploration methods. MESA J., South Australia, pp. 34–39.

Hubbard, B.E., Crowley, J.K., 2005. Mineral mapping on the Chilean–Bolivian Altiplano using co-orbital ALI, ASTER and Hyperion imagery: data dimensionality issues and solutions. Remote Sens. Environ. 99 (1–2), 173–186.

Hunt, G.R., Salisbury, J.W., 1970. Visible and near infrared spectra of minerals and rocks: I silicate minerals. Mod. Geol. 1, 283–300.

IAEA-TECDOC-1363, 2003. Guidelines for radioelement mapping using Gamma ray spectrometry data. International Atomic Energy Agency, Austria, ISBN 92–0–108303–3, ISSN 1011-4289.

Jain, M., Tandon, S.K., Bhatt, S.C., 2004. Late quaternary stratigraphic development in the lower Luni, Mahi and Sabarmati river basins, western India. Proc. Indian Acad. Sci.-Earth Planet. Sci. 113 (3), 453–471.

Jobbágy, V., Chmielewska, I., Kovács, T., Chałupnik, S., 2009. Uranium determination in water samples with elevated salinity from Southern Poland by micro coprecipitation using alpha spectrometry. Microchem. J. 93, 200–205.

Kavak, K.S., 2005. Recognition of gypsum geohorizons in the Sivas Basin (Turkey) using ASTER and Landsat ETM+ images. Int. J. Remote Sens. 26 (20), 4583–4596.

Kochhar, N., 1989. High heat producing granites ofthe Malani igneous suite, northern peninsular India. Indian Minerals 43, 339–346.

Kochhar, N., 2000. Attributes and significance of the A-type Malani Magmatism, northwestern peninsular India; Crustal evaluation and metallogeny in the northwestern peninsular India, Narosa, New Delhi.

Kruse, F.A., 1996. Identification and mapping of minerals in drill core using hyperspectral image analysis of infrared reflectance spectra. Int. J. Remote Sens. 17 (9), 1623–1632.

Kruse, F.A., Lefkoff, A.B., Boardman, J.W., Heidebrecht, K.B., Shapiro, A.T., Barloon, P.J., Goetz, A.F.H., 1993. The spectral image-processing system (SIPS)—interactive visualisation and analysis of imaging spectrometer data. Remote Sens. Environ. 44, 145–163.

Kumar, A., Rout, S., Narayanan, U., Mishra, M.K., Tripathi, R.M., Singh, J., Kumar, S., Kushwaha, H.S., 2011. Geochemical modelling of uranium speciation in the subsurface aquatic environment of Punjab State in India. J. Geol. Mining Res. 3 (5), 137–146.

Kusuma, K.N., Ramakrishnan, D., Pandalai, H.S., Kailash, G., 2010. Noise reduction in field spectroradiometer data – the "noise-signal index threshold" and its significance in hyperspectral image classification: a case study of laterite, lateritic-bauxite and bauxite mapping. Geocarto Int. 25 (7), 569–580.

Kusuma, K.N., Ramakrishnan, D., Pandalai, H.S., 2012. Spectral pathways for effective delineation of high-grade bauxites: a case study from the Savitri River Basin, Maharashtra, India, using EO-1 Hyperion data. Int. J. Remote Sens. 33 (22), 7273–7290.

Lagacherie, P., Baret, F., Feret, J.B., Netto, J.M., Robbez-Masson, J.M., 2007. Estimation of soil clay and calcium carbonate using laboratory, field and airborne hyperspectral measurements. Remote Sens. Environ. 112, 825–835.

Lévesque, J., Neville, R.A., Staenz, K., 2001. Preliminary results on the investigation of hyperspectral remote sensing for the identification of uranium mine tailings. Canadian Nuclear Safety Commission, 280 Slater, Ottawa, Ontario, Canada, K1P 5S9.

Please cite this article in press as: Bharti, R., et al. Spectral pathways for exploration of secondary uranium: An investigation in the desertic tracts of Rajasthan and Gujarat, India. Adv. Space Res. (2015), http://dx.doi.org/10.1016/j.asr.2015.07.015

Leybourne, M.I., Cameron, E.M., 2007. Groundwaters in geochemical exploration: methods, applications, and future directions. In: Advances in Regional-Scale Geochemical Methods, Fifth Decennial International Conference on Mineral Exploration, pp. 201–221.

Lorber, A., Harel, A., Goldbart, Z., Brenner, I.B., 1987. Curve resolution and figures of merit estimation for determination of trace elements in geological materials by inductively coupled plasma atomic emission spectrometry. Anal. Chem. 59, 1260–1266.

Maithani, P.B., Banerjee, R., Gurjar, R., 2015. Geochemistry and petrogenesis of radioactive lamprophyres associated with Erinpura granites around Isra, Sirohi district, Rajasthan. Explor. Res. At. Minerals (EARFAM), 1–18.

Mann, A.W., Deutscher, R.L., 1978. Genesis principles for the precipitation of Carnotite in calcrete drainages in Western Australia. Econ. Geol. 73, 1724–1737.

Mann, A.W., Horwitz, R.C., 2007. Groundwater calcrete deposits in Australia some observations from Western Australia. J. Geol. Soc. Aust.: Int. Geosci. J. Geol. Soc. Aust. 26 (5–6), 293–303.

Martínez-Montoya, J.F., Herrero, J., Casterad, M.A., 2010. Mapping categories of gypseous lands in Mexico and Spain using Landsat imagery. J. Arid Environ. 74, 978–986.

Middleton, W.G., 1984. An assessment of the use of hydrogeochemistry in exploration for calcrete uranium in Australia. Report of the Working Group on Uranium Geology Organized by the International Atomic Energy Agency, Vienna, IAEA-TECDOC-322.

Misra, A., Pande, D., Kumar, K.R., Nanda, L.K., Maithani, P.B., Chaki, A., 2011. Calcrete-hosted surficial uranium occurrence in playa-lake environment at Lachhri, Nagaur District, Rajasthan, India. Curr. Sci. 101 (1), 84–88.

Noble, R.R.P., Gray, D.J., Reid, N., 2011. Regional exploration for channel and playa uranium deposits in Western Australia using groundwater. Appl. Geochem. 26 (12), 1956–1974.

Perkins, T., Adler-Golden, S., Matthew, M., Berk, A., Anderson, G., Gardner, J., Felde, G., 2005. Retrieval of atmospheric properties from hyper- and multispectral imagery with the FLAASH atmospheric correction algorithm. Proc. SPIE 5979, 59790E.

Perkins, T., Adler-Golden, S.M., Cappelaere, P., Mandl, D. 2012. High-speed atmospheric correction for spectral image processing. In: SPIE Optical Engineering, XVIII, 83900V.

Raghuwanshi, S.S., 1992. Airborne gamma-ray spectrometry in uranium exploration. Adv. Space Res. 12 (7), 77–86.

Ramakrishnan, D., Tiwari, K.C., 2006. Calcretized-ferricretes around Jaisalmer area, Thar Desert, India: their chemistry, mineralogy, micromorphology and genesis. Turk. J. Earth Sci. 15 (2), 1–13.

Ramakrishnan, D., Nithya, M., Singh, K.D., Bharti, R., 2013. A field technique for rapid lithological discrimination and ore mineral identification: Results from Mamandur Polymetal Deposit. India. Journal of Earth System Sciences 122 (1), 1–14.

Ramesh Kumar, K., Pande, D., Misra, A., Nanda, L.K., 2011. Playa Sediments of the Didwana Lake, Rajasthan: A New Environment for Surficial-type Uranium Mineralisation in India. Journal geological society of India. 77, 89–94.

Ranjbar, H., Honarmand, M., Moezifar, Z., 2004. Application of the Crosta technique for porphyry copper alteration mapping, using ETM+ data in the southern part of the Iranian volcanic sedimentary belt. J. Asian Earth Sci. 24, 237–243.

Salisbury J.W., 1998. Spectral measurements field guide, Unpublished report; U.S. Defense Technology Information Center Report, ADA362372 82.

San, B.T., Suzen, M.L., 2010. Evaluation of different atmospheric correction algorithms for EO-1 Hyperion imagery. In: International Archives of the Photogrammetry, Remote Sensing and Spatial Information Science, vol. XXXVIII, Part 8, Kyoto, Japan, pp. 392–397.

Sinha, R., Stueben, D., Berner, Z., 2004. Palaeohydrology of the Sambhar playa, Thar desert, India, using geomorphological and sedimentological evidences. J. Geol. Soc. India 64, 419–430.

So, P.T.C., Dong, C.Y., 2002. Fluorescence Spectrophotometry. Encyclopedia of life Sciences. Macmillan Publishers Ltd, Nature Publishing Group, pp. 1–4.

Stamnes, K., Tsay, S.C., Wiscombe, W., Jay-aweera, K., 1988. Numerically Stable Algorithm for Discrete-Ordinate-Method Radiative Transfer in Multiple Scattering and Emitting Layered Media. Appl. Opt. 27, 2502–2509.

Sundaram, B., Feitz, A.J., Caritat, P., de Plazinska, A., Brodie, R.S., Coram, J., Ransley, T., 2009. Groundwater Sampling and Analysis–A Field Guide. Geoscience Australia, Record 2009 (27), 95.

Tangestani, M.H., Moore, F., 2000. Iron oxide and hydroxyl enhancement using the Crosta Method: a case study from the Zagros Belt, Fars Province. Iran. International Journal of Applied Earth Observation and Geoinformation 2 (2), 140–146.

Tosheva, Z., Stoyanova, K., Nikolchev, L., 2004. Comparison of different methods for uranium determination in water. J. Environ. Radioact. 72, 47–55.

Tsurikov, N., 2009. Uranium exploration-safety, environmental, social and regulatory considerations. Calytrix Consulting Pvt. Ltd.

Väisänen, A., Matilainen, R., Tummavuori, J., 2000. The determination of certain major and minor elements in geological samples by inductively coupled plasma atomic emission spectrometry. Some interference problems with the analysis of geological standard reference materials and nutrition supplements. Fresenius. J. Anal. Chem. 367 (8), 755–760.

Van-der-Meer, F., 2004. Analysis of spectral absorption features in hyperspectral imagery. Int. J. Appl. Earth Obs. Geoinf. 5, 55–68.

Veselsky, J.C., Kwiecinska, B., Wehrstein, E., Suschny, O., 1988. Determination of Uranium in Minerals by Laser Fluorimetry. Analyst 113, 451–455.

Waterwatch, 2005. Australia National Technical Manual. Module-6 Groundwater Monitoring. Department of the Environment and Heritage, Canberra.

Zhang, Jie-lin, 2008. Hyperspectral data mining for characterising granite type uranium deposits in south china. In: The International Archives of the Photogrammetry, Remote Sensing and Spatial Information Sciences, vol. XXXVII, Part B8, Beijing.

Please cite this article in press as: Bharti, R., et al. Spectral pathways for exploration of secondary uranium: An investigation in the desertic tracts of Rajasthan and Gujarat, India. Adv. Space Res. (2015), http://dx.doi.org/10.1016/j.asr.2015.07.015